Localized pattern formation for mussel-algae model and other reaction-diffusion systems with saturation

Shuangquan Xie,[1] Theodore Kolokolnikov,[2] and Juncheng Wei[3]

[1] *Department of Mathematics*
Hunan University
*Changsha, Hunan, China**
[2] *Department of Mathematics and Statistics*
Dalhousie University
Halifax, N.S., Canada†
[3] *Department of Mathematics*
Chinese University of Hong Kong
Shatin, NT, Hong Kong‡

Abstract. We examine a class of reaction-diffusion systems where saturation drives pattern pattern formation. A prime example is the classical model of mussel-algae interactions. We asymptotically construct a pattern consisting of N spikes. Unlike many other models where the inner spike profile is described by a *nonlinear* ODE $w''-w+w^p=0$, here it is described by a *linear* ODE $w''+w-1=0$. We then study the stability of resulting patterns. A new non-local eigenvalue problem (NLEP) is derived which controls the structural stability of N such spikes. We rigorously prove its stability in the relevant regime, taking advantage of the explicit formula for the shape of the spike. Self-replication is also observed, and we derive a new "core problem" which captures this phenomenon. Finally, the asymptotic stability band for existence of N spikes is given. Our methods are applicable to a wide range of systems that exhibit saturation; we provide a variant of Schnakenberg model as another example. Numerical simulations confirm our asymptotic predictions.

1. INTRODUCTION

In this paper we examine localized patterns for some reaction-diffusion systems driven by saturation or allee effects. These are often included in population models in order to account for the effect of population size on predation or nutrient consumption. Consider the well-known model of mussel-algae interactions [1–4]:

$$M_t = d_1 M_{xx} - \frac{k_1}{k_2+k_3 M} M + k_4 AM, \qquad A_t = d_2 A_{xx} + k_5 - k_6 A - k_7 AM. \tag{1.1}$$

The mussel death rate $\frac{k_1}{k_2+k_3M}$ decreases with higher density, reflecting a "strength in numbers" protection mechanism. The path to pattern formation through Turing bifurcation is well understood for this and related models. In particular the saturation is essential for formation of spatial patterns in (1.1) (no spatial patterns are possible when $k_3=0$). Our goal here is to study localized patterns that arise far from the Turing bifurcation threshold. This is in contrast to numerous existing studies of this model, where the patterns are typically studied close to the Turing bifuraction threshold. We note that the same model but with $k_6=0$ was studied in e.g. [5, 6] from the point of view of chemical reactions with a saturation.

Many models of vegetation patterns incorporate saturation for both nutrients and plant biomass [7–9]. Among the simplest examples, consider the following variant of the classical Klausmeier model:

$$v_t = d_2 v_{xx} - k_4 v + \frac{k_5 v}{k_6 v + k_7} vu, \quad u_t = d_1 u_{xx} + k_1 - k_2 u - k_3 uv. \tag{1.2}$$

Here, v represents the biomass density and v the density of water. The water absorbtion rate by the plants $\frac{k_5 v}{k_6 v+k_7}$ is assumed to saturate with increased biomass density.

Both of these models have complex spatial patterns made up of spikes, as illustrated in Figures 1, 5. We are interested in certain limits of the models (1.2) and (1.1) where the saturation plays a key role. As with most other studies of spike patterns, the basic building block is the asymptotic profile of the spike. In almost all other studies,

* xieshuangquan2013@gmail.com
† tkolokol@gmail.com (corresponding author); T.K. is supported by NSERC, Canada.
‡ wei@math.cuhk.edu.hk; J. Wei is partially supported by National Key R&D Program of China (No. 2022YFA1005602), and Hong Kong General Research Fund "New frontiers in singular limits of nonlinear partial differential equations.

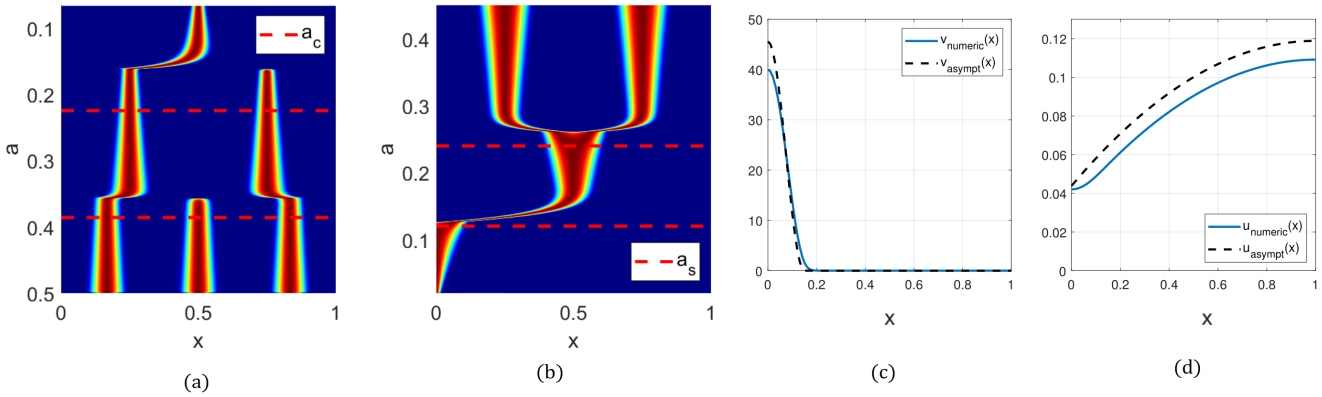

FIG. 1. (a) Spike competiton instability for the model (2.1). Here, $D = 1$, $\varepsilon = 0.0015$, and a is gradually decreased according to $a = 0.5 - 10^{-5}t$. Dashed line a_c shows the asymptotic threshold given by (2.25) (b) Self-replication. Parameters are same as in (a) except a is gradually increased according to $a = 0.02 + 10^{-5}t$. Asymptotic for a_s given by (2.24) is also shown. (c-d) Half-spike steady state of (2.2), which is a basic building block of patterns. Here, $a = 0.15$, $\varepsilon = 0.01$, $l = 1$. Dashed lines indicate asymptotics (2.10).

this profile satisfies a *nonlinear* ODE of the form $w_{yy} - w + w^p = 0$, whose explicit solution is given by a power of sech. By contrast, when saturation dominates, we find a new *linear* ODE for the ground state in the inner region, of the form $w_{yy} + w - 1 = 0$. This is then matched to the outer region to construct the full spike profile.

As we will see later, saturation can have a profound effect on the resulting spatial patterns. The original paper of Klausmeier [10] assumed no saturation ($k_6 = 0$ in (1.2)). In this case the model (1.2) is equivalent the Gray-Scott model or the Schnakenberg model (when $k_2 = 0$) which has been intensively studied from the point of view of localized patterns. There is a large literature on the subject; we refer to the book [11] and references therein for review.

Similar spot patterns have been studied in many other reaction-diffusion models. Some prominent examples include Gray-Scott model [12–17] the Schnakenberg model [18–20], vegetation patches in arid environments [10, 21–25], a model of crime hot-spots in a model of residential burglaries [26–29] and animal skin patterns [30–35]. We single out the paper [36] which is the first to give the full description of stability of N spikes for the related Gierer-Meinhardt model. The framework developed in that paper forms the basis for stability analysis in this work.

The summary of the paper is as follows. Section 2 is dedicated to the analysis of the model (1.1). We construct the equilibrium spike profile in §2.1. We then study the stability of a pattern consisting of N identical copies of a spike in §2.2. As in the classical analysis [36], there are two types of eigenvalues to consider: large eigenvalues which correspond to structural stability of the pattern, and small eigenvalues that arise due to translation invariance of the inner region and are related to slow spike dynamics. We find a novel non-local eigenvalue problem (NLEP) (3.1) which describes the stability of spikes with respect to large eigenvalues, and prove their (in)stability depending on problem parameters. We then derive small-eigenvalue instability thresholds directly, by constructing asymmetric spike patterns. As with other models, we find that the competition instability – responsible for spike death – is triggered due to small eigenvalue instabilities. In §2.3 we describe derive the so-called core problem which captures the spike self-replication observed in (1.1). The stability of NLEP problem is analysed rigorously in §3. Section 4 is devoted to a similar analysis for the model (1.2). We conclude with discussion and open problems in 5.

2. MUSSEL-ALGAE MODEL

We illustrate our technique on the Mussel-Algae model (1.1). Simulations of the steady state (see Figure 1) show the existence of spike patterns, corresponding to localized concentrations of mussel population. To simplify the calculation and illustrate key points, we will assume that the natural death rate of algae is negligible compared to death due to mussel consumption; $k_4 \ll k_5$. Moreover, we assume that the algae population changes on a faster timescale than the mussel population. With these assumuptions, after some rescaling we write the model in the form

$$v_t = \varepsilon^2 v_{xx} + uv - \frac{v}{1+v}; \quad 0 = Du_{xx} + a - uv. \tag{2.1}$$

Here, v is the rescaled M, and u is the rescaled A; the zero on the left hand side of the second equation reflects the assumption that the mussel population grows on a much slower time scale than the aglae.

2.1. Steady state.

Let us first construct a spiky steady state for the model (2.1). It satisfies

$$0 = \varepsilon^2 v_{xx} + uv - \frac{v}{1+v}; \quad 0 = Du_{xx} + a - uv. \tag{2.2}$$

A typical steady state is shown in Figure 1(c,d). We start by constructing a steady state consisting of a half-spike on the domain $[0, l]$. By even reflections, this can be extended to N symmetric interior spikes on the domain $(-l, (2N-1)l)$ of size $L = 2Nl$.

The steady state is divded into two regions: the *inner* region inside the spike and the outer region (refer to Figure 1(c,d)). In the inner region, we freeze $u \sim u_0$, where u_0 is to be determined. We look for solution of the form

$$v \sim \frac{1}{u_0} V(z), \qquad z = \frac{\sqrt{u_0}}{\varepsilon} x. \tag{2.3}$$

Equation for $V(z)$ then becomes

$$V_{yy} + V - \frac{V}{u_0 + V} = 0. \tag{2.4}$$

The first integral of (2.4) reads

$$\frac{V_y^2}{2} + \frac{V^2}{2} - V - u_0 \log(V/u_0 + 1) = 0. \tag{2.5}$$

where we assumed $V(y) \to 0$ as $y \to \pm\infty$.

We look for solution to (2.4) in the limit $u_0 \to 0$. Let $V_{\max} = \max V(z)$. Then equation (2.4) becomes

$$V_{yy} + V - 1 \sim 0 \tag{2.6}$$

and from (2.5) we obtain $V_{\max} \sim 2$. Consequently, we obtain $V \sim 1 + \cos(y)$. The approximation (2.6) breaks down when $V = O(u_0)$, in other words, when $y \sim \pi$; an additional boundary layer near $y = \pi$ exists to resolve the transition from (2.6) to (2.5). We obtain the spike profile of the form

$$v(x) \sim \frac{1}{u_0} \begin{cases} 1 + \cos\left(\frac{\sqrt{u_0}}{\varepsilon} x\right), & 0 \le x < \pi \frac{\varepsilon}{\sqrt{u_0}} \\ 0, & \text{otherwise} \end{cases}. \tag{2.7}$$

To obtain u_0 we integrate equation for u in (2.1) to obtain $al \sim u_0 \int_0^l v \sim \frac{\varepsilon}{\sqrt{u_0}} \pi$, so that

$$u_0 \sim \left(\frac{\varepsilon \pi}{la}\right)^2. \tag{2.8}$$

In the outer region, $v \sim 0$ so we have

$$u \sim u_0 - \frac{a}{2D}\left((x-l)^2 - l^2\right). \tag{2.9}$$

In summary, the half-spike on domain $[0, l]$ has the profile

$$v(x) \sim \left(\frac{al}{\varepsilon\pi}\right)^2 \begin{cases} 1 + \cos\left(\frac{\pi}{al} x\right), & 0 \le x < al \\ 0, & \text{otherwise} \end{cases}; \qquad u_0 \sim \left(\frac{\varepsilon\pi}{la}\right)^2 - \frac{a}{2D}(x - l). \tag{2.10}$$

The assumption $v \gg 1$ then implies $a \gg \varepsilon$; at the same time for the spike to be localized we must also have also have $a \ll 1$. Figure 1(c,d) shows the comparison between the asymptotics (2.10) and the full steady state as obtained by numerical simulations.

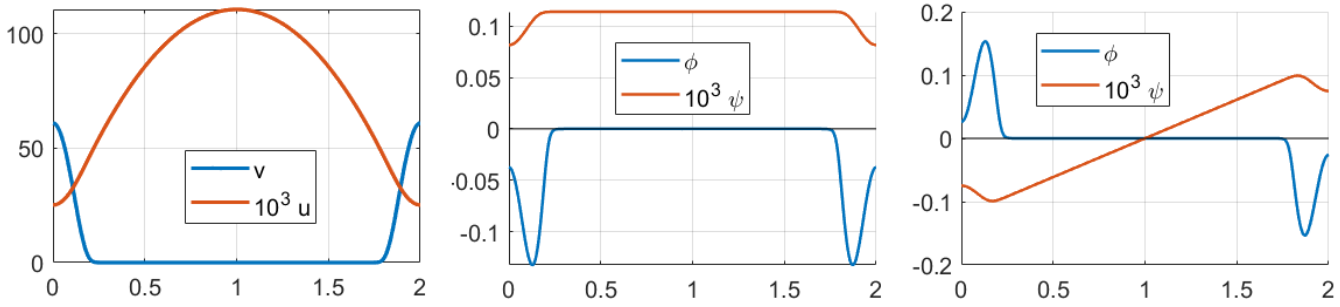

FIG. 2. Left: Steady state consisting of two boundary spikes. Middle: even eigenfunction corresponding to BC $\phi'(l) = 0$. Right: odd eigenfunction corresponding to BC $\phi(l) = 0$.

2.2. Stability

Half-spike. We start by studying the stability of a single boundary half-spike on domain of size $(0, l)$. Linearize around the steady state constructed above as follows:

$$v(x,t) = v(x) + \phi(x)e^{\lambda t}, \quad u(x,t) = u(x) + \psi(x)e^{\lambda t}$$

to obtain

$$\lambda\phi = \varepsilon^2\phi_{xx} + \phi u + \psi v - \left(\frac{1}{1+v}\right)^2\phi; \qquad 0 = D\psi_{xx} - \phi u - \psi v. \tag{2.11}$$

In the inner region $y = x\frac{\sqrt{u_0}}{\varepsilon}$ we approximate $\psi \sim \psi_0 = \psi(0)$, $\phi(x) = \Phi(y)$ and $v \sim \frac{1}{u_0}V(y)$. We obtain,

$$\lambda_0\Phi \sim \Phi_{yy} + \Phi + \frac{V}{u_0^2}\psi_0, \quad \lambda_0 = \lambda/u_0,\ V(y) = 1 + \cos y, \quad y \in [0,\pi]. \tag{2.12}$$

To match to the outer solution where $\phi \sim 0$, we impose a point constraint

$$\Phi(\pi) = 0.$$

We intergrate the equation for ψ in (4.15) to obtain ψ_0 :

$$\psi_0 \sim -\frac{u_0^2}{\pi}\int_0^\pi \Phi(y)dy.$$

This yields the following *non-local eigenvalue problem* (NLEP):

$$\begin{cases} \lambda_0\Phi = \Phi_{yy} + \Phi - \kappa\,(1+\cos y)\int_0^\pi \Phi(y)dy, \\ \Phi'(0) = 0; \qquad \Phi(\pi) = 0. \end{cases} \tag{2.13}$$

where $\kappa = \frac{1}{\pi}$. The probelm (2.13) is studied rigorously in §3. In particular, Theorem 3.1 states that the eigenvalues are stable ($\mathrm{Re}\,(\lambda_0) \le 0$ for all λ_0) as long as $\kappa \ge \kappa_0 = \frac{2}{3\pi}$, and are unstable otherwise. Here, $\kappa = \frac{1}{\pi} > \frac{2}{3\pi}$. This proves that a single boundary spike is stable.

Two boundary spikes. Next, consider the configuration consisting of two boundary on domain $[0, 2l]$ as illustrated in Figure 2. This configuration admits two distinct eigenvalues, depending on the parity of the eigenfunction with respect to the center of the domain, as illustrated in Figure 2. If the eigenfunction is even with respect to the center, this is equivalent to the stability of a single half-spike on the domain $[0, l]$ and was shown to be stable. On the other hand, odd eigenfunction is equivalent to solving the eigenvalue problem (4.15) with boundary conditions $\psi(\pm l) = 0 = \phi(\pm l)$. The inner problem for Φ is the same (2.13); but now $\phi_0 = \phi(0)$ satisfies

$$\psi_{xx} = 0; \qquad \psi(l) = 0, \quad D\psi'(0^+) = \frac{\varepsilon}{\sqrt{u_0}}\left(u_0\int_0^\pi \Phi dy + \psi_0\frac{\pi}{u_0}\right)$$

We obtain $\psi(x) = \psi'(0)(x-l)$, $\psi_0 \sim -l\psi'(0^+)$ so that

$$\psi_0 = -l^2 \frac{a}{D\pi} \left(u_0 \int_0^\pi \Phi dy + \psi_0 \frac{\pi}{u_0} \right). \tag{2.14}$$

We then obtain the problem (2.13) but with

$$\kappa = \frac{1}{\pi} \frac{D^{-1} l^4 a^3 (\varepsilon\pi)^{-2}}{1 + D^{-1} l^4 a^3 (\varepsilon\pi)^{-2}}. \tag{2.15}$$

The stability boundary corresponds to setting $\kappa = \kappa_0 = \frac{2}{3\pi}$, corresponding to the threshold $D^{-1} l^4 a^3 (\varepsilon\pi)^{-2} = 2$, or $a = a_c$ where

$$a_c = \varepsilon^{2/3} D^{1/3} l^{-4/3} 2^{1/3} \pi^{2/3}. \tag{2.16}$$

When $a > a_c$, the two boundary spikes are stable, and they are unstable when $a < a_c$.

Multiple interior spikes. Next we consider N spikes on the domain of size $L = 2lN$, with periodic boundary conditions. We fix the domain $x \in [-l, (2l-1)N]$ and put the spikes at locations $x = 2lk, k = 0..N-1$. There are small and large eigenvalues to compute [11, 36].

Small eigenvalues. We start with the small eigenvalues that correspond to translational modes. Instead of the full computation of the small eigenvalues, we will short-circuit the process and only compute asymmetric spike solutions following [28, 37]. The point where asymmetric branch bifurcates off the symmetric configuration corresponds to the simultaneous zero-crossing of $N-1$ small eigenvalues [37].

From (2.10), we have:

$$u(l) \sim u_0 + \frac{a}{2D} l^2 \sim \left(\frac{\varepsilon\pi}{a}\right)^2 \frac{1}{l^2} + \frac{a}{2D} l^2$$

The function $l \to u(l)$ attains a minimum when

$$-2 \left(\frac{\varepsilon\pi}{a}\right)^2 \frac{1}{l^3} + \frac{a}{D} l = 0.$$

Solving for a, we obtain the same formula as in (2.16). This is precisely the bifurcation point of zero-crossing of small eignevalues, at which all N small eigenvalues cross zero simultaneously [37]. This shows that the stability threshold of two interior boundary spikes on domain of size $4l$ (due to small eigenvalues) is exact same as the stability threshold of two boundary spikes on the domain of size $2l$ (due to large eigenvalues). It is notable that the classical systems such as GM or Schankenberg models exhibit exactly the same equality of stability thresholds. Finally, we let $l = L/(2N)$ to obtain the threshold for N spikes on domain of size L. The small eignevalues are all stable when $a > a_c$ and are all unstable when $a < a_c$.

Large eigenvalues. To compute large eigenvalues on the periodic domain, we consider the eigenvalue problem (2.11) but subject to the "Floquet" BC:

$$\psi(l) = e^{i\theta}\psi(-l), \quad \psi'(l) = e^{i\theta}\psi'(-l)$$

and similar for ϕ. Extend ψ on entire domain by setting $\psi(x) = e^{i\theta}\psi(x-2l)$. Then $\psi((2l-1)N) = e^{i\theta N}\psi(-l)$. By choosing

$$\theta = 2\pi m/N, \quad m = 0 \ldots N-1,$$

we obtain periodic BC on entire domain. It remains to solve for ψ_0. This is equivalent to solving

$$\begin{cases} \psi'' = c\boldsymbol{\delta}(x) \\ \psi(l) = e^{i\theta}\psi(-l), \quad \psi'(l) = e^{i\theta}\psi'(-l) \end{cases} \tag{2.17}$$

where

$$c = 2l \frac{a}{D\pi} \left(u_0 \int_0^\pi \Phi dy + \psi_0 \frac{\pi}{u_0} \right)$$

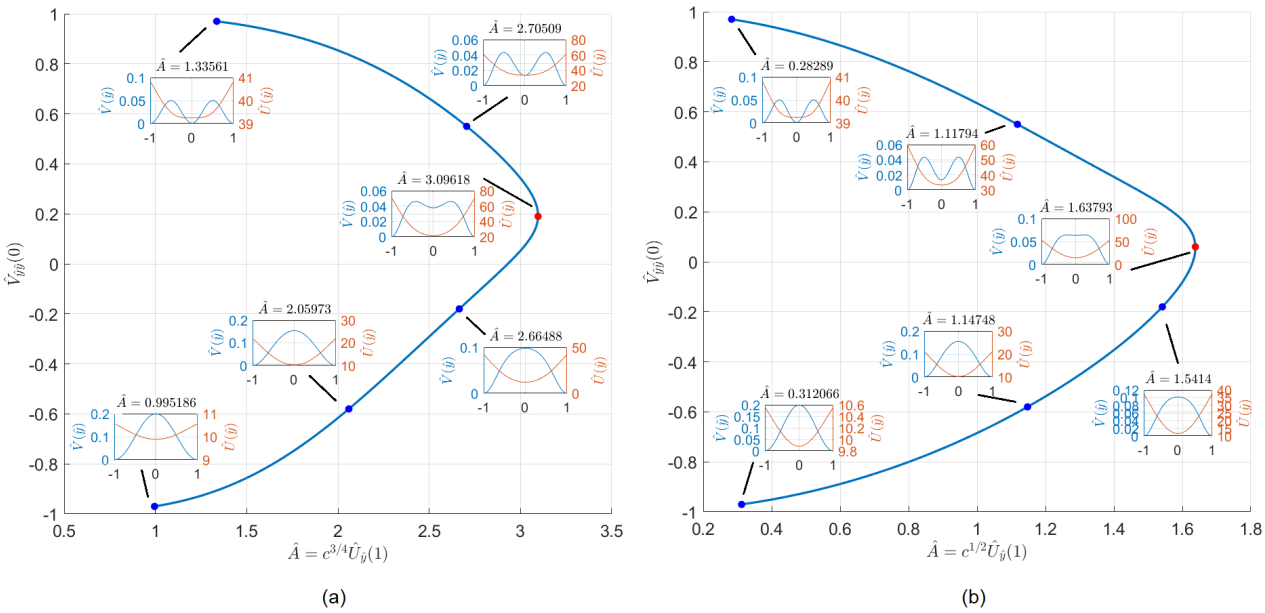

FIG. 3. (a) Bifurcation diagram for the core problem (2.23). There is a fold point at $\hat{A} = \hat{A}_s = 3.0918$ which is responsible for self-replication. (b) Bifurcation diagram for the core problem (4.19). The fold point is at $\hat{A} = \hat{A}_s = 1.6379$.

This is equivalent to solving $\psi'' = 0$ with jump condition $\psi'(0^+) - \psi'(0^-) = c$ and continuity condition $\psi(0^+) = \psi(0^-)$. After some algebra we find that

$$\psi(0) = \frac{cl}{\cos(\theta) - 1} = -\frac{cl}{2\sin^2(\theta/2)}. \tag{2.18}$$

We then obtain (2.13) with the premultiplier κ being equal to

$$\kappa = \frac{1}{\pi} \frac{\left(D\sin^2(\theta/2)\right)^{-1} l^4 a^3 (\varepsilon\pi)^{-2}}{1 + \left(D\sin^2(\theta/2)\right)^{-1} l^4 a^3 (\varepsilon\pi)^{-2}}. \tag{2.19}$$

Setting $\kappa = 2/3/\pi$ yields the critical threshold

$$a_m = a_c \sin^{2/3}\left(\frac{2\pi m}{N}\right). \tag{2.20}$$

where a_c is given in (2.25). Note that $\alpha_m \le a_c$ for all m, so that all of the thresholds a_m are below the threshold a_c that triggers the small eigenvalues. In this sense, the situation is the same as for the Schnakenberg and other related models: the instability is first triggered by small eignevalues, as a is decreased.

2.3. Self-replication

Next we study the phenomenon of spike self-replication. This phenomenon is observed in numerous other reaction-diffusion models. See for example [12, 13, 16, 17, 38–43] and references therein. The path to self-replication corresponds to a disappearance of the steady state via a fold-point bifurcation [38]. At the bifurcation point, there there is typically the so-called "core problem" [12, 17, 39, 40] near the spike center which must be solved numerically, then matched to the outer region. Near the fold point, the solution branch connects a single spike to a double-spike structure. As we now show, a similar structure (but with a somewhat different core problem) occurs for model (2.1).

We start by looking for at the inner region of the spike located at $x = 0$. Rescale:

$$x = ay, \quad u = \varepsilon^2 a^{-2} U, \quad v = \varepsilon^{-2} a^2 V, \quad D_0 = D\varepsilon^2 a^{-4}.$$

Assuming v large, the leading-order inner problem becomes

$$V_{yy} - 1 + UV = 0, \quad D_0 U_{yy} - UV \sim 0. \tag{2.21}$$

The inner problem for $V(y)$ is defined for $y \in [0, R]$ where R is the inner domain length that is necessary to solve for. In order to match to the outer region, we impose boundary conditions

$$V'(0) = 0 = U'(0); \quad V(R) = 0 = V'(R);$$

The matching condition is obtained by integrating equation for U in (2.21). We have: $U'(R) = \frac{1}{D_0}\int_0^R UV dy \sim \frac{1}{aD_0}\int_0^l uv dx$. On the other hand, integrating (2.2) we have $\int_0^l uv = al$. We thus obtain the matching condition

$$U_y(\infty) = l/D_0. \tag{2.22}$$

Together, equations (2.21, 2.22) form a closed system that determines V, U as well as R as a function of system parameters. Next, we further scale to remove R as follows:

$$y = R\hat{y}, \quad V = R^2\hat{V}, \quad U = R^{-2}\hat{U}$$

to arrive at the problem

$$\hat{V}_{yy} - 1 + \hat{U}\hat{V} = 0, \quad c\hat{U}_{\hat{y}\hat{y}} - \hat{U}\hat{V} = 0 \tag{2.23a}$$

where $c = D\varepsilon^2 a^{-4} R^{-4}$. The boundary conditions become

$$\hat{V}'(0) = 0 = \hat{U}'(0); \quad \hat{V}(1) = 0 = \hat{V}'(1). \tag{2.23b}$$

Condition (2.22) then becomes $\hat{U}_{\hat{y}}(1) = R^3 l/D_0$. Eliminating R, we get $\hat{U}_{\hat{y}}(1) = c^{-3/4} l D^{-1/4} \varepsilon^{-1/2} a$.

Let $\hat{A} = c^{3/4}\hat{U}_{\hat{y}}(1)$. The matching then becomes

$$\hat{A} := c^{3/4}\hat{U}_{\hat{y}}(1) = lD^{-1/4}\varepsilon^{-1/2} a. \tag{2.23c}$$

Numerically, we find that the system (2.23) has a fold point at $\hat{A} = \hat{A}_s \approx 3.0962$. This is illustrated in Figure 3(a), where we plot $\hat{A}$ versus $\hat{V}_{yy}(0)$. The two branches connect a single spike to a double spike solution and are responsible for self-replication observed in the numerics. When $\hat{A}$ is increased past $\hat{A}_s$ the steady state is lost and self-replication occurs.

We summarize the results as follows.

Proposition 2.1. *Consider a symmetric $N-$spike pattern for the model (2.1) on the domain of size L, and let $l = L/(2N)$. Let*

$$a_s = \varepsilon^{1/2} D^{1/4} l^{-1} \hat{A}_s \text{ where } \hat{A}_s \approx 3.0962, \tag{2.24}$$

$$a_c = \varepsilon^{2/3} D^{1/3} l^{-4/3} 2^{1/3} \pi^{2/3}. \tag{2.25}$$

When $N \geq 2$, the $N-$spike pattern is stable when $a \in (a_c, a_s)$. Self-replication is triggered when a increases past a_s and competition (spike death) is triggered when a decreases past a_c. When $N = 1$, a single spike is stable when $\varepsilon \ll a < a_s$.

3. NONLOCAL EIGENVALUE PROBLEM

Here, we rigorously study the stability of the key NLEP problem (2.13):

$$\begin{cases} \lambda_0 \Phi = \Phi_{yy} + \Phi - \kappa w \int_0^\pi \Phi(y) dy, \qquad w(y) = 1 + \cos(y) \\ \Phi'(0) = 0; \qquad \Phi(\pi) = 0. \end{cases} \tag{3.1}$$

We have the following characterization of stability for the operator (3.1).

Theorem 3.1. *Let $\kappa_0 = \frac{2}{3\pi}$. The following thresholds phenomenon holds:*

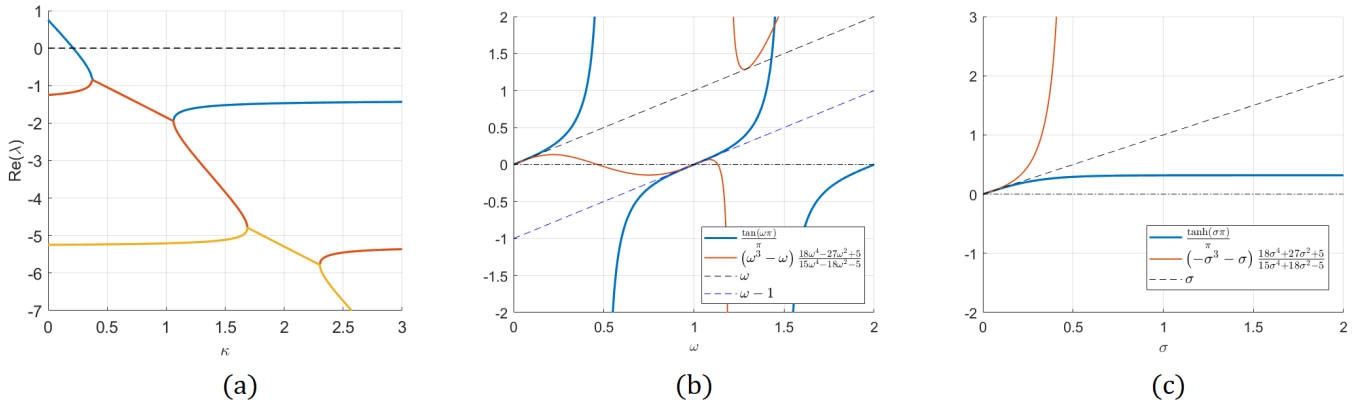

FIG. 4. (a) Spectrum of the eigenvlue problem (3.1) computed numerically. Note the zero-crossing at $\kappa = \kappa_0 = \frac{2}{3\pi}$ of the principal eigenvalue. The problem is stable for $\kappa_0 > \frac{2}{3\pi}$, despite having complex eigenvalues (b) Plot of (3.3). (c) Plot of (3.4).

- *If $\kappa > \kappa_0$, then all eigenvalues of (3.1) are strictly stable, i.e.* $\mathrm{Re}\,(\lambda_0) < 0$ *for all* λ_0.
- *If $\kappa = \kappa_0$, then there exists one zero eigenvalue and the rest of eigenvalues are strictly stable,* $\mathrm{Re}\,(\lambda_0) < 0$.
- *Suppose that $\kappa < \kappa_0$. Then there exists a real positive eigenvalue $\lambda_0 > 0$.*

Note that the operator in (3.1) is not self-adjoint and in general the eigenvalues can be complex, which complicates the analysis. We will follow the ideas of the method introduced in [44]. The idea is to "self-adjointize" the operator.

In what follows, we write $\int = \int_0^\pi dy$. Let w_0, κ_0 be the solution to to (3.1) corresponding to the zero eigenvalue, namely

$$w_0'' + w_0 - \kappa_0 w \int w_0 = 0.$$

Explicitly, we have

$$w_0 = \cos y + 1 + \frac{1}{2} y \sin y; \quad \kappa_0 = \frac{1}{\int w_0} = \frac{2}{3\pi}.$$

Now define the operator

$$L_1 \Phi := \Phi'' + \Phi - \kappa_0 w \int \Phi - \kappa_0 \int w\Phi + \kappa_1 \int \Phi \tag{3.2}$$

where κ_1 is chosen such that $L_1 w_0 = 0$:

$$0 = -\kappa_0 \int w w_0 + \kappa_1 \int w_0,$$
$$\kappa_1 = \kappa_0 \frac{\int w w_0}{\int w_0} = \frac{5}{6\pi}.$$

Lemma 3.2. *The operator L_1 is self-adjoint, and non-positive definite.*

Proof. An explicit computation shows that the eigenvalues of L_1 satisfy

$$\frac{\tan(\omega\pi)}{\pi} = (\omega^3 - \omega)\frac{18\omega^4 - 27\omega^2 + 5}{15\omega^4 - 18\omega^2 - 5}, \quad \lambda = 1 - \omega^2 \tag{3.3}$$

Since L_1 is self-adjoint, λ is purely real. So there are two cases to consider: either ω is purely real or it is purely imaginary.

Case 1, ω is purely real. The graph of lhs and rhs of (3.3) is shown in Figure 4(b). As can be seen from the graph, there are no roots when $\omega \in (0, 1)$. This is easy to prove rigorously as follows. Let $f(\omega) = rhs(3.3)$. Then

for $\omega \in (0,1)$, $f(\omega)$ is below the line $y=\omega$ and above the line $y=\omega-1$. Indeed, a simple computation shows $f(\omega)=\omega$ is equivalent $\left(3\omega^2-5\right)^2=0$ which has no roots in $(0,1)$. Similarly, setting $f(w)=\omega-1$ one obtains $18\omega^4+54\omega^3+48\omega^2+15\omega+5=0$, which again has no roots for $\omega>0$ as all the coefficients are positive.

Case 2, $\omega=i\sigma$ with σ purely real. Then equation (3.3) becomes

$$\frac{\tanh(\sigma\pi)}{\pi}=\left(-\sigma^3-\sigma\right)\frac{18\sigma^4+27\sigma^2+5}{15\sigma^4+18\sigma^2-5} \tag{3.4}$$

The graph of (3.4) is shown in Figure 4(c) and shows that there are no non-zero solutions to (3.4). This is easily shown using the same arguments as in Case 1 (and is left to the reader). This completes the proof of the lemma. ■

We are now ready to prove Theorem **3.1.**

Proof of Theorem 3.1

To show the instability when $\kappa<\kappa_0$, we solve (3.1) explicitly to find that λ_0 satisfies

$$\frac{\tan(\omega\pi)}{\pi\left(\omega-\omega^3\right)}=1-\frac{\omega^2}{\kappa\pi},\quad \lambda_0=1-\omega^2. \tag{3.5}$$

Simple calclulus shows that (3.5) has a root $\omega\in(0,1)$ when $\kappa<\kappa_0$ (in fact $\omega=1$ corresponds to $\kappa=\kappa_0$). This shows the existence of a positive (and real) eigenvalue of (3.1) when $\kappa<\kappa_0$.

Next we show stability when $\kappa\geq\kappa_0$. Write (3.1) as

$$\lambda_0\Phi=L_1\Phi+(\kappa_0-\kappa)\,w\int\Phi+\kappa_0\int w\Phi-\kappa_1\int\Phi$$

Decompose $\lambda_0=\lambda_R+i\lambda_I,\quad \Phi=\Phi_R+i\Phi_I$; so that

$$\lambda_R\Phi_R-\lambda_I\Phi_I=L_1\Phi_R+(\kappa_0-\kappa)\,w\int\Phi_R+\kappa_0\int w\Phi_R-\kappa_1\int\Phi_R \tag{3.6}$$

$$\lambda_R\Phi_I+\lambda_I\Phi_R=L_1\Phi_I+(\kappa_0-\kappa)\,w\int\Phi_I+\kappa_0\int w\Phi_I-\kappa_1\int\Phi_I \tag{3.7}$$

The combination $\int\Phi_R\int(3.6)+\int\Phi_I\int(3.7)$ yields:

$$\begin{aligned}\lambda_R\left\{\left(\int\Phi_R\right)^2+\left(\int\Phi_I\right)^2\right\}&=\left\{\int\Phi_RL_1\Phi_R+\Phi_IL_1\Phi_I\right\}+(\kappa_0-\kappa-\kappa_1)\,\pi\left\{\left(\int\Phi_R\right)^2+\left(\int\Phi_I\right)^2\right\}\\&+\kappa_0\pi\left\{\int\Phi_Rw\int\Phi_R+\int\Phi_Iw\int\Phi_I\right\}\end{aligned} \tag{3.8}$$

Note that

$$\int w\left(\Phi''+\Phi\right)=\int\Phi\left(w''+w\right)=\int\Phi.$$

Multiplying (3.6, 3.7) w, integrating and eliminating λ_I therefore yields

$$\lambda_R\left\{\left(\int w\Phi_R\right)^2+\left(\int w\Phi_I\right)^2\right\}=\left(1-\kappa\int w^2\right)\left\{\int\Phi_Rw\int\Phi_R+\int\Phi_Iw\int\Phi_I\right\}. \tag{3.9}$$

Eliminate $\int w\Phi_R\int\Phi_R+\int w\Phi_I\int\Phi_I$ between (3.8) and (3.9) to obtain

$$\lambda_R(A)-\kappa_0\pi\lambda_RB\frac{1}{\left(1-\kappa\int w^2\right)}=\left\{\int\Phi_RL_1\Phi_R+\Phi_IL_1\Phi_I\right\}+(\kappa_0-\kappa-\kappa_1)\,\pi A$$

where

$$A=\left\{\left(\int\Phi_R\right)^2+\left(\int\Phi_I\right)^2\right\},\quad B=\left\{\left(\int\Phi_Rw\right)^2+\left(\int\Phi_Iw\right)^2\right\}.$$

Using the fact that $\int w^2=1/\kappa_0$, we get

$$\lambda_R\left(A+\frac{4}{9\pi}\frac{1}{\kappa-\kappa_0}B\right)=\left\{\int\Phi_RL_1\Phi_R+\Phi_IL_1\Phi_I\right\}+(\kappa_0-\kappa-\kappa_1)\,\pi A$$

Now $A,B>0$ whereas the right hand side is always negative when $\kappa>\kappa_0$. This shows $\lambda_R<0$ whenever $\kappa>\kappa_0$. ■

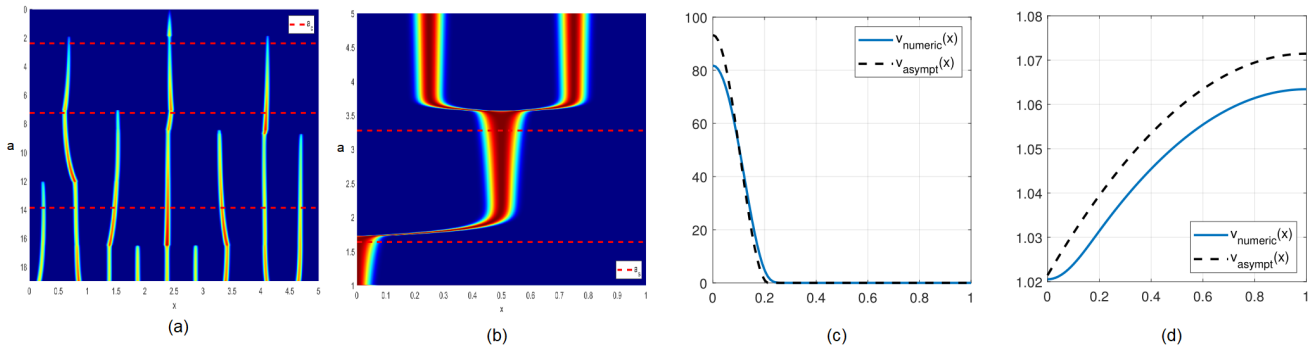

FIG. 5. (a) Competition instability for model (4.10). Here, $D = 100, \varepsilon = 0.0025$, $L = 5$, and a is gradually decreased according to $a = 20(1 - 10^{-5}t)$. Dashed lines indicate the asymptotic prediction a_c (4.21) for $N = 9, 6$, and 3 spikes (b) Spike self-replication. Here, $d = 1, L = 1, \varepsilon = 0.005$. Dashed lines indicate the asymptotic prediction a_s (4.20) for $N = 1/2$ and $N = 1$ spikes. (c-d) Half-spike steady state of (4.10). Here, $d = 100$, $a = 10$, $\varepsilon = 0.01$, $l = 1$. Dashed lines indicate asymptotics (4.11, 4.12, 4.13).

4. SCHANKENBERG MODEL WITH SATURATION

We now perform a similar analysis for the Schnakenberg model with saturation (1.2). After some scalings, we write it in the form

$$v_t = \varepsilon^2 v_{xx} - v + \frac{v}{1+v}uv, \qquad 0 = Du_{xx} + a - uv. \tag{4.10}$$

We simplified the model assuming k_2 is negligible, and further assumed that the plant population changes on a slower scale than the precipitation in the soil (hence zero instead of u_t). We first construct the steady state, then analyse its stability.

As before, we will assume that u and v decouple in the inner region, and start by constructing a single boundary spike on domain $[0, l]$. In the inner region, u is assumed to be nearly constant, and turns out to be very close to 1, whereas v is large. Setting $u(x) \sim 1 + \delta$, where δ is a small constant to be determined, the equilibrium for v becomes

$$0 = \varepsilon^2 v_{xx} + \delta v + (1+\delta)\left(-1 + \frac{1}{1+v}\right).$$

Assuming v large we estimate $(1+\delta)\left(-1+\frac{1}{1+v}\right) \sim -1$. We then find, as in §2,

$$v(x) \sim \frac{1}{\delta}\begin{cases} \left(1 + \cos\left(x\frac{\sqrt{\delta}}{\varepsilon}\right)\right), & |x| < \pi\frac{\varepsilon}{\sqrt{\delta}} \\ 0, & |x| > \pi\frac{\varepsilon}{\sqrt{\delta}} \end{cases} \tag{4.11}$$

To find δ, we integrate $\int_0^l (a - uv)dx = 0$ which yields

$$\delta = \varepsilon^{2/3}\left(\frac{\pi}{al}\right)^{2/3}. \tag{4.12}$$

Stability computation is also very similar to §2. We compute that

$$u(x) \sim 1 + \delta - \frac{a}{2D}(x-l)^2 + \frac{a}{2D}l^2, \quad \delta^{2/3} \ll x < l \tag{4.13}$$

so that

$$u(l) = 1 + \delta + \frac{a}{2D}l^2 \sim 1 + \varepsilon^{2/3}\left(\frac{\pi}{a}\right)^{2/3} l^{-2/3} + \frac{a}{2D}l^2.$$

The function $l \to u(l)$ attains a minimum when

$$\frac{2}{3}\varepsilon^{2/3}\left(\frac{\pi}{a}\right)^{2/3} l^{-5/3} = 2\frac{a}{2D}l. \tag{4.14}$$

Solving (4.14) for a, we obtain the stability threshold $a = a_c$ given by (4.21). The pattern is unstable if $a < a_c$ and is is stable for $a > a_c$. For large eigenvalues, we linearize around the steady state to obtain the eigenvalue problem

$$\lambda\phi = \varepsilon^2\phi_{xx} + \phi\left((u-1) - \frac{u}{(1+v)^2}\right) + \left(-1 + v + \frac{1}{1+v}\right)\psi, \quad 0 = D\psi_{xx} - \phi u - \psi v. \tag{4.15}$$

The corresponding NLEP problem is identical to (2.13) but with the following κ :

$$\kappa = \frac{1}{\pi}\varepsilon^{-2/3}\left(\frac{\pi}{al}\right)^{-2/3} \text{ for a single boundary spike on } (0,l)$$
$$\kappa = \frac{l^2 a}{D}\frac{1}{\pi}\varepsilon^{-2/3}\left(\frac{\pi}{al}\right)^{-2/3} \text{ for double boundary spike on } (0,2l)$$
$$\kappa = \frac{l^2 a}{D\sin^2(\theta/2)}\frac{1}{\pi}\varepsilon^{-2/3}\left(\frac{\pi}{al}\right)^{-2/3}, \ m = 1\ldots N-1 \text{ for } N \text{ spikes on domain of size } 2lN.$$

As before, the stability boundary corresponds to $\kappa = \kappa_0 = \frac{2}{3\pi}$. So no surprise here: we have the usual situation that the small eigenvalues are destabilized before large ones, and therefore (4.21) gives the competition instability threshold.

Finally, we derive the self-replication thresholds. We rescale,

$$u(x) = 1 + \varepsilon^{2/3}U(y), \quad v(x) = \frac{1}{\varepsilon^{2/3}}V(y), \quad x = \varepsilon^{2/3}y.$$

We then obtain, at leading order, a coupled *core problem*

$$V_{yy} + VU - 1 = 0, \qquad DU_{yy} - V = 0. \tag{4.16}$$

Similar to (2.21), the inner problem for $V(y)$ is defined for $y \in [0,R]$ where R is the inner domain length that is necessary to solve for through additional constraints

$$V'(0) = 0 = U'(0) \quad \text{and} \quad V(R) = V'(R) = 0. \tag{4.17}$$

The matching condition is obtained integrating equation for U in (4.16). We have: $U'(R) = \frac{1}{D}\int_0^R V(y)dy \sim \frac{1}{D}\int_0^l v(x)dx$. On the other hand, integrating (4.10) we have $\int_0^L uv \sim \int_0^L v = al$. We thus obtain the matching condition

$$U'(R) = \frac{al}{D}. \tag{4.18}$$

Together, equations (4.16, 4.17, 4.18) form a closed system that determines V, U as well as R as a function of system parameters. Next, we further scale to remove R as follows:

$$y = R\hat{y}, \quad V = R^2\hat{V}, \quad U = \frac{1}{R^2}\hat{U}, \quad c = \frac{D}{R^6}.$$

The resulting system is

$$\hat{V}_{\hat{y}\hat{y}} + \hat{V}\hat{U} - 1 = 0, \qquad c\hat{U}_{\hat{y}\hat{y}} - \hat{V} = 0; \tag{4.19a}$$
$$\hat{V}'(0) = 0 = \hat{U}'(0); \qquad \hat{V}(1) = \hat{V}'(1) = 0 \tag{4.19b}$$

whereas equation (4.18) becomes

$$\hat{A} = \hat{U}'(1)\sqrt{c}, \quad \text{where } \hat{A} = \frac{al}{\sqrt{D}}. \tag{4.19c}$$

For each c, the system (4.19) is solved numerically. Numerically, we find a fold point at $\hat{A} = \hat{A}_s = 1.638$. This is illustrated in Figure 3, where we plot $\hat{A}$ versus $\hat{V}_{yy}(0)$. The two branches connect a single spike to a double spike solution and are responsible for self-replication observed in the numerics.

We summarize the results as follows.

Main Result 4.1. *Consider a symmetric $N-$spike pattern for the model (4.10) on the domain of size L, and let $l = L/(2N)$. Let*

$$a_s = D^{1/2} l^{-1} \hat{A}_{\max} \text{ where } \hat{A}_s \approx 1.638, \tag{4.20}$$

$$a_c = D^{3/5} \varepsilon^{2/5} l^{-8/5} (2/3)^{3/5} \pi^{2/5}. \tag{4.21}$$

When $N \geq 2$, the $N-$spike pattern is stable when $a \in (a_c, a_s)$. Self-replication is triggered when a increases past a_s and competition (spike death) is triggered when a decreases past a_c. When $N = 1$, a single spike is stable when $\varepsilon \ll a < a_s$.

5. DISCUSSION

We studied the effect of saturation on localized pattern formation for systems (1.1), (1.2). To our knowledge, this is the first time that the asymptotics and stability of localized patterns have been studied for the Mussel-Algae model 1.1). In contrast to numerous previous studies where the spike have a profile of the form of sech to some power, the spike studied here has a cosine-type profile (2.10) and leads to novel NLEP problem (3.1).

Our techniques apply to a wide range of reaction-diffusion systems in the presence of saturation. Another example is a variant of Macarthur–Rosenzweig type model with an Allee effect for the predator, similar to [45]:

$$N_t = d_1 N_{xx} + k_1 N - k_2 N^2 - k_3 NP, \qquad P_t = d_2 P_{xx} - k_4 P + \frac{k_5 P}{k_6 P + k_7} NP \tag{5.22}$$

Here, N and P are populations of prey and predator, respectively. The predator-prey interactions are modulated by the predator allee effect $\frac{k_5 P}{k_6 P + k_7}$, which allows for spatial pattern formation. It is very similar to the model (1.2) except that the constant production is replaced by a logistic growth term. This makes the outer problem non-linear. It would be interesting to study how this changes the dynamics and stability of localized patterns.

There are numerous open questions for future study. These include: spot dynamics, oscillatory instabilities and construction of stripes and spots in higher dimensions. In two dimensions, we expect the spot profile to be described by a Bessel J function. It would be interesting to extend the stability analysis of §2.2 to this context. On the other hand, stable stripe solutions have also been observed in numerical simulations of Mussel-Algae model in 2D when the drift terms are added to algae [3]. It was shown in [46] that drift can indeed lead to stripe stabilization for classical Schnakenberg model. It would be interesting to attempt a similar analysis for the Mussel-Algae model.

[1] J. v. d. Koppel, M. Rietkerk, N. Dankers, P. M. Herman, Scale-dependent feedback and regular spatial patterns in young mussel beds, The American Naturalist 165 (3) (2005) E66–E77.

[2] R.-H. Wang, Q.-X. Liu, G.-Q. Sun, Z. Jin, J. van de Koppel, Nonlinear dynamic and pattern bifurcations in a model for spatial patterns in young mussel beds, Journal of the Royal Society Interface 6 (37) (2009) 705–718.

[3] Q.-X. Liu, E. J. Weerman, P. M. Herman, H. Olff, J. van de Koppel, Alternative mechanisms alter the emergent properties of self-organization in mussel beds, Proceedings of the royal society B: biological sciences 279 (1739) (2012) 2744–2753.

[4] R. A. Cangelosi, D. J. Wollkind, B. J. Kealy-Dichone, I. Chaiya, Nonlinear stability analyses of turing patterns for a mussel-algae model, Journal of Mathematical Biology 70 (2015) 1249–1294.

[5] J. Ibanez, M. Velarde, Multiple steady states in a simple reaction–diffusion model with michaelis–menten (first-order hinshelwood–langmuir) saturation law: The limit of large separation in the two diffusion constants, Journal of Mathematical Physics 19 (1) (1978) 151–156.

[6] R. Peng, J. Shi, M. Wang, On stationary patterns of a reaction–diffusion model with autocatalysis and saturation law, Nonlinearity 21 (7) (2008) 1471.

[7] M. Rietkerk, M. C. Boerlijst, F. Van Langevelde, R. HilleRisLambers, J. v. de Koppel, L. Kumar, H. H. Prins, A. M. de Roos, Self-organization of vegetation in arid ecosystems, The American Naturalist 160 (4) (2002) 524–530.

[8] V. Guttal, C. Jayaprakash, Self-organization and productivity in semi-arid ecosystems: Implications of seasonality in rainfall, Journal of theoretical biology 248 (3) (2007) 490–500.

[9] Z. Ge, The hidden order of turing patterns in arid and semi-arid vegetation ecosystems, Proceedings of the National Academy of Sciences 120 (42) (2023) e2306514120.

[10] C. A. Klausmeier, Regular and irregular patterns in semiarid vegetation, Science 284 (5421) (1999) 1826–1828.

[11] J. Wei, M. Winter, Mathematical aspects of pattern formation in biological systems, Vol. 189, Springer Science & Business Media, 2013.

[12] J. E. Pearson, Complex patterns in a simple system, Science 261 (5118) (1993) 189–192.

[13] W. N. Reynolds, S. Ponce-Dawson, J. E. Pearson, Self-replicating spots in reaction-diffusion systems, Physical Review E 56 (1) (1997) 185.

[14] A. Doelman, T. J. Kaper, P. A. Zegeling, Pattern formation in the one-dimensional gray-scott model, Nonlinearity 10 (2) (1997) 523.

[15] C. Muratov, Theory of domain patterns in systems with long-range interactions of coulomb type, Physical Review E 66 (6) (2002) 066108.

[16] Y. Nishiura, D. Ueyama, Spatio-temporal chaos for the gray–scott model, Physica D: Nonlinear Phenomena 150 (3) (2001) 137–162.

[17] T. Kolokolnikov, M. J. Ward, J. Wei, The existence and stability of spike equilibria in the one-dimensional gray–scott model: the pulse-splitting regime, Physica D: Nonlinear Phenomena 202 (3-4) (2005) 258–293.

[18] D. L. Benson, P. K. Maini, J. A. Sherratt, Unravelling the turing bifurcation using spatially varying diffusion coefficients, Journal of Mathematical Biology 37 (5) (1998) 381–417.

[19] D. Iron, J. Wei, M. Winter, Stability analysis of turing patterns generated by the schnakenberg model, Journal of mathematical biology 49 (2004) 358–390.

[20] T. Kolokolnikov, J. Wei, Pattern formation in a reaction-diffusion system with space-dependent feed rate, SIAM Review 60 (3) (2018) 626–645.

[21] J. A. Sherratt, An analysis of vegetation stripe formation in semi-arid landscapes, Journal of mathematical biology 51 (2) (2005) 183–197.

[22] J. A. Sherratt, G. J. Lord, Nonlinear dynamics and pattern bifurcations in a model for vegetation stripes in semi-arid environments, Theoretical population biology 71 (1) (2007) 1–11.

[23] Y. Chen, T. Kolokolnikov, J. Tzou, C. Gai, Patterned vegetation, tipping points, and the rate of climate change, European Journal of Applied Mathematics 26 (06) (2015) 945–958.

[24] C. Gai, T. Kolokolnikov, Resource-mediated competition between two plant species with different rates of water intake, SIAM Journal on Applied Mathematics 83 (2) (2023) 576–602.

[25] F. Al Saadi, A. Champneys, C. Gai, T. Kolokolnikov, Spikes and localised patterns for a novel schnakenberg model in the semi-strong interaction regime, European Journal of Applied Mathematics 33 (1) (2022) 133–152.

[26] M. B. Short, M. R. D'ORSOGNA, V. B. Pasour, G. E. Tita, P. J. Brantingham, A. L. Bertozzi, L. B. Chayes, A statistical model of criminal behavior, Mathematical Models and Methods in Applied Sciences 18 (supp01) (2008) 1249–1267.

[27] J. R. Zipkin, M. B. Short, A. L. Bertozzi, Cops on the dots in a mathematical model of urban crime and police response, to appear, DCDS-S (supplement) (2014).

[28] T. Kolokolnikov, M. J. Ward, J. Wei, The stability of steady-state hot-spot patterns for a reaction-diffusion model of urban crime., Discrete & Continuous Dynamical Systems-Series B 19 (5) (2014).

[29] S. Chaturapruek, J. Breslau, D. Yazdi, T. Kolokolnikov, S. G. McCalla, Crime modeling with lévy flights, SIAM Journal on Applied Mathematics 73 (4) (2013) 1703–1720.

[30] S. Kondo, R. Asai, et al., A reaction-diffusion wave on the skin of the marine angelfish pomacanthus, Nature 376 (6543) (1995) 765–768.

[31] R. Barrio, C. Varea, J. Aragón, P. Maini, A two-dimensional numerical study of spatial pattern formation in interacting turing systems, Bulletin of mathematical biology 61 (3) (1999) 483–505.

[32] P. K. Maini, T. E. Woolley, R. E. Baker, E. A. Gaffney, S. S. Lee, Turing's model for biological pattern formation and the robustness problem, Interface focus (2012) rsfs20110113.

[33] D. Dalle Nogare, A. B. Chitnis, Self-organizing spots get under your skin, PLoS Biology 15 (12) (2017) e2004412.

[34] A. N. Landge, B. M. Jordan, X. Diego, P. Müller, Pattern formation mechanisms of self-organizing reaction-diffusion systems, Developmental biology 460 (1) (2020) 2–11.

[35] E. Grall, P. Tschopp, A sense of place, many times over-pattern formation and evolution of repetitive morphological structures, Developmental Dynamics 249 (3) (2020) 313–327.

[36] D. Iron, M. J. Ward, J. Wei, The stability of spike solutions to the one-dimensional gierer–meinhardt model, Physica D: Nonlinear Phenomena 150 (1) (2001) 25–62.

[37] M. J. Ward, J. Wei, The existence and stability of asymmetric spike patterns for the schnakenberg model, Studies in Applied Mathematics 109 (3) (2002) 229–264.

[38] Y. Nishiura, D. Ueyama, A skeleton structure of self-replicating dynamics, Physica D: Nonlinear Phenomena 130 (1) (1999) 73–104.

[39] C. Muratov, V. V. Osipov, Static spikeautosolitons in the gray-scott model, Journal of Physics A: Mathematical and General 33 (48) (2000) 8893.

[40] A. Doelman, T. J. Kaper, L. A. Peletier, Homoclinic bifurcations at the onset of pulse self-replication, Journal of Differential Equations 231 (1) (2006) 359–423.

[41] T. Kolokolnikov, M. Tlidi, Spot deformation and replication in the two-dimensional belousov-zhabotinski reaction in a water-in-oil microemulsion, Physical review letters 98 (18) (2007) 188303.

[42] T. Kolokolnikov, M. J. Ward, J. Wei, Spot self-replication and dynamics for the schnakenburg model in a two-dimensional domain, Journal of nonlinear science 19 (1) (2009) 1–56.

[43] C.-C. Chen, T. Kolokolnikov, Simple pde model of spot replication in any dimension, SIAM Journal on Mathematical Analysis 44 (5) (2012) 3564–3593.

[44] J. Wei, On single interior spike solutions of the gierer–meinhardt system: uniqueness and spectrum estimates, European Journal of Applied Mathematics 10 (4) (1999) 353–378.

[45] S. K. Akhtar, A. B. Peet, E. Peacock-Lopez, Complex dynamics in a modified macarthur–rosenzweig model with predator

paring, Journal of Biological Systems 20 (01) (2012) 87–108.
[46] T. Kolokolnikov, M. Ward, J. Tzou, J. Wei, Stabilizing a homoclinic stripe, Philosophical Transactions of the Royal Society A: Mathematical, Physical and Engineering Sciences 376 (2135) (2018) 20180110.